Angewandte Chemie
Eine Zeitschrift der Gesellschaft Deutscher Chemiker

Supporting Information

Perylene π-Bridges Equally Delocalize Anions and Cations: Proportioned Quinoidal and Aromatic Content

Paula Mayorga Burrezo[+], Wangdong Zeng[+], Michael Moos, Marco Holzapfel, Sofia Canola, Fabrizia Negri, Concepciò Rovira, Jaume Veciana, Hoa Phan, Jishan Wu,* Christoph Lambert, and Juan Casado**

anie_201905657_sm_miscellaneous_information.pdf

Content

1. Synthesis and characterization of 1

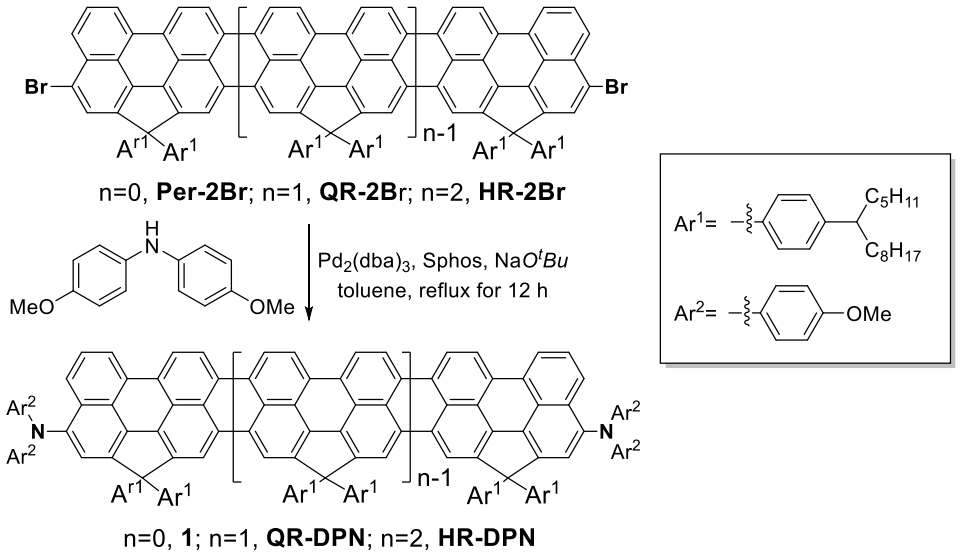

Scheme S1. Synthesis of the bis(amino)rylenes by C-N coupling reaction.

Per-2Br, **QR-2Br** and **HR-2Br** were prepared according to our previously reported paper (Zeng, W.; Hong, Y.; Medina Rivero, S.; Kim, J.; Zafra, J. L.; Phan, H.; Gopalakrishna, T. Y.; Herng, T. S.; Ding, J.; Casado, J.; Kim, D.; Wu, J. Stable Nitrogen-centered Bis(imino)rylene Diradicaloids. *Chem. Eur. J.* **2018**, *24*, 4944–4951).

Compound **1**: A two-necked round bottom flask was charged with **Per-2Br** (200 mg, 0.207 mmol), $Pd_2(dba)_3$ (15.18 mg, 16.6 μmol, 0.08 equiv), Sphos (21 mg, 0.052 mmol, 0.25 equiv), bis(4-methoxyphenyl)amine (190 mg, 0.81 mmol, 4 equiv) and NaO^{t}Bu (96.7 mg, 1.10 mmol, 5 equiv). The mixture was degassed and stirred at 110 °C for 12h under argon. The solution was cooled down to room temperature and the organic layer was washed by water, dried over anhydrous $MgSO_4$. The solvent was removed under vacuum and the residue was purified by column chromatography (silica gel, hexane/DCM = 4/1) to afford the desired product **1** as a red solid (248 mg, 90% yield). ^{1}H NMR ($CDCl_3$, 500 MHz): δ ppm 8.06 (d, *J* = 7.38 Hz, 2H), 7.66 (d, *J* = 8.46 Hz, 2H), 7.43 (s, 2H), 7.35 (t, *J* = 7.38 Hz, 2H), 7.15 (d, *J* = 8.20 Hz, 2H), 7.00 (m, 8H), 6.91 (d, *J* = 8.22 Hz, 2H), 6.75 (m, 8H), 3.77 (s, 12H), 2.38 (br, 2H), 1.57-1.53 (m, 8H), 1.27-1.10 (m, 42H), 0.86-0.81 (m, 12H); HR-MS (APCI): *m*/*z* = 1263.7906, calcd. for $C_{89}H_{103}N_2O_4$ (M+1): *m*/*z* = 1263.7912, error = 0.50 ppm.

QR-DPN: A two-necked round bottom flask was charged with **QR-2Br** (184 mg, 0.104 mmol), $Pd_2(dba)_3$ (7.59 mg, 8.3 μmol, 0.08 equiv), Sphos (10.5 mg, 0.026 mmol, 0.25 equiv), bis(4-methoxyphenyl)amine (95 mg, 0.40 mmol, 4 equiv) and NaO^{t}Bu (48.3 mg, 0.55 mmol, 5 equiv). The mixture was degassed and stirred at 110 °C for 12h under argon. The solution was then slowly cooled down to room temperature and the organic layer was washed by water, dried over anhydrous $MgSO_4$. The solvent was removed under vacuum and the residue was purified by column chromatography (silica gel, hexane/DCM = 4/1) to afford the desired product **QR-DPN** as a blue solid (180 mg, 84%). ^{1}H NMR ($CDCl_3$, 500 MHz): δ ppm 8.83 (br, 2H), 8.36 (br, 2H), 8.26 (d, *J* = 8.10 Hz, 2H), 8.14 (br, 2H), 7.59 (br, 2H), 7.38 (d, *J* = 8.20 Hz, 12H), 7.00 (d, *J* = 8.30 Hz, 8H), 6.99 (m, 8H), 6.75 (d, *J* = 8.80 Hz, 8H), 3.72 (s, 12H), 2.47 (br, 4H), 1.60 (br, 8H), 1.51 (br, 8H), 1.30-1.20 (br, 72H), 8.82-0.80 (br, 24H); HR-MS (APCI): *m*/*z* = 2068.3558, calcd. for $C_{150}H_{175}N_2O_4$ (M+1): *m*/*z* = 2068.3546, error = -0.50 ppm.

HR-DPN: A two-necked round bottom flask was charged with **HR-2Br** (100 mg, 0.039 mmol), $Pd_2(dba)_3$ (2.8 mg, 3.1 μmol, 0.08 equiv), Sphos (4 mg, 0.01 mmol, 0.25 equiv), bis(4-methoxyphenyl)amine (36 mg, 0.155 mmol, 4 equiv) and NaO^{t}Bu (18.8 mg, 0.194 mmol, 5 equiv). The mixture was degassed and stirred at 110 °C for 12h under argon.

The solution was then slowly cooled down to room temperature and the organic layer was washed by water, dried over anhydrous $MgSO_4$. The solvent was removed under vacuum and the residue was purified by column chromatography (silica gel, hexane/DCM = 2/1) to afford the desired product **HR-DPN** as a green solid (91 mg, 82%). ^1H NMR ($CDCl_3$, 500 MHz): 9.11 (br, 2H), 9.64 (br, 2H), 8.53 (br, 2H), 8.49 (br, 2H), 8.40 (br, 2H), 8.38 (br, 2H), 8.35 (br, 2H), 8.29 (br, 2H), 8.12 (br, 2H), 7.84 (br, 2H), 7.69-7.59 (m, 8H), 7.49-7.35 (m, 12H), 7.07-6.94 (m, 12H), 6.84-7.86 (m, 8H), 6.53 (br, 2H), 2.43 (m, 6H), 1.68-1.60 (m, 24H), 1.36-1.08 (m, 108H), 0.91-0.79 (m, 36H); HR-MS (APCI): *m*/*z* = 2871.9051, calcd. for $C_{211}H_{246}N_2O_4$ (M): *m*/*z* = 2871.9102, error =1.80 ppm.

Appendix: NMR spectra and HR mass spectra of all new compounds

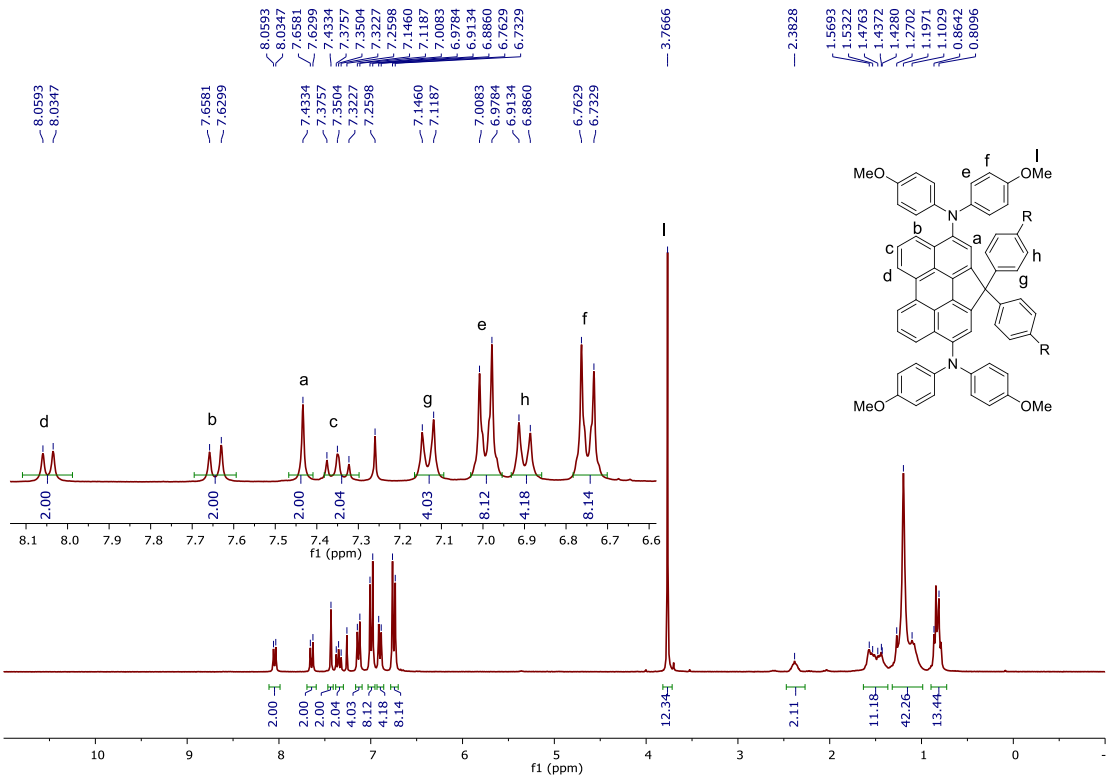

Figure S1. ^{1}H NMR spectrum of compound **1** (300 MHz, $CDCl_3$, rt).

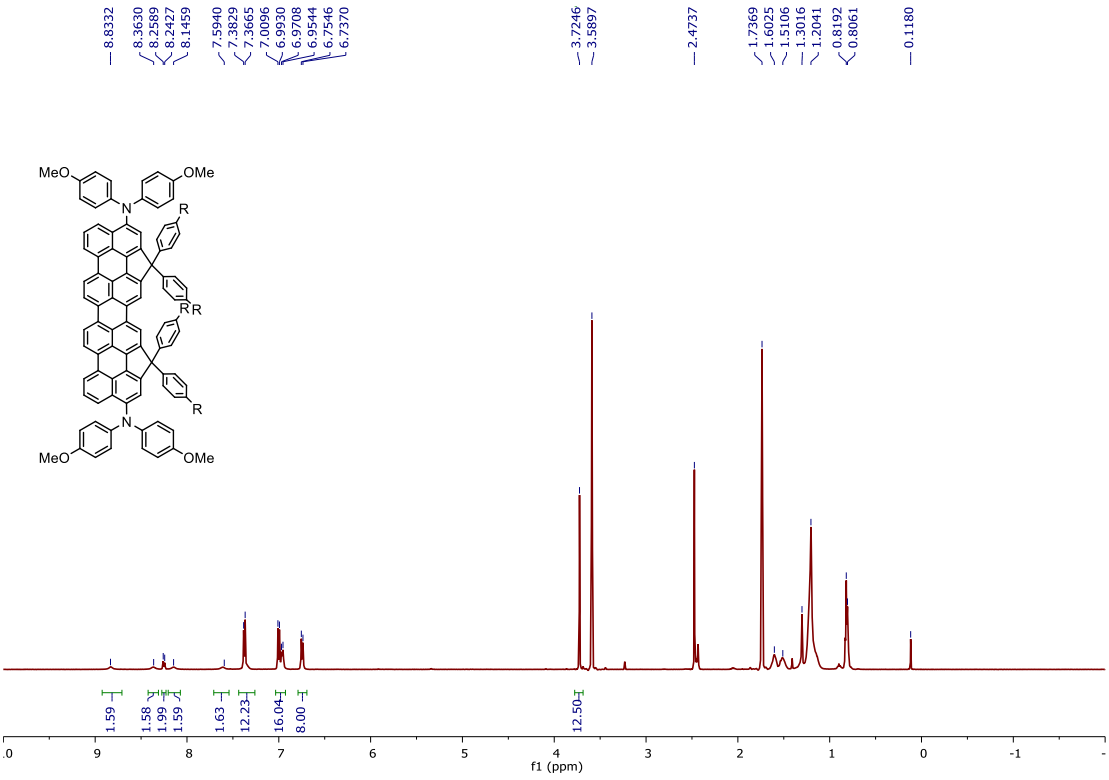

Figure S2. ^{1}H NMR spectrum of compound **QR-DPN** (500 MHz, d_8-THF, rt).

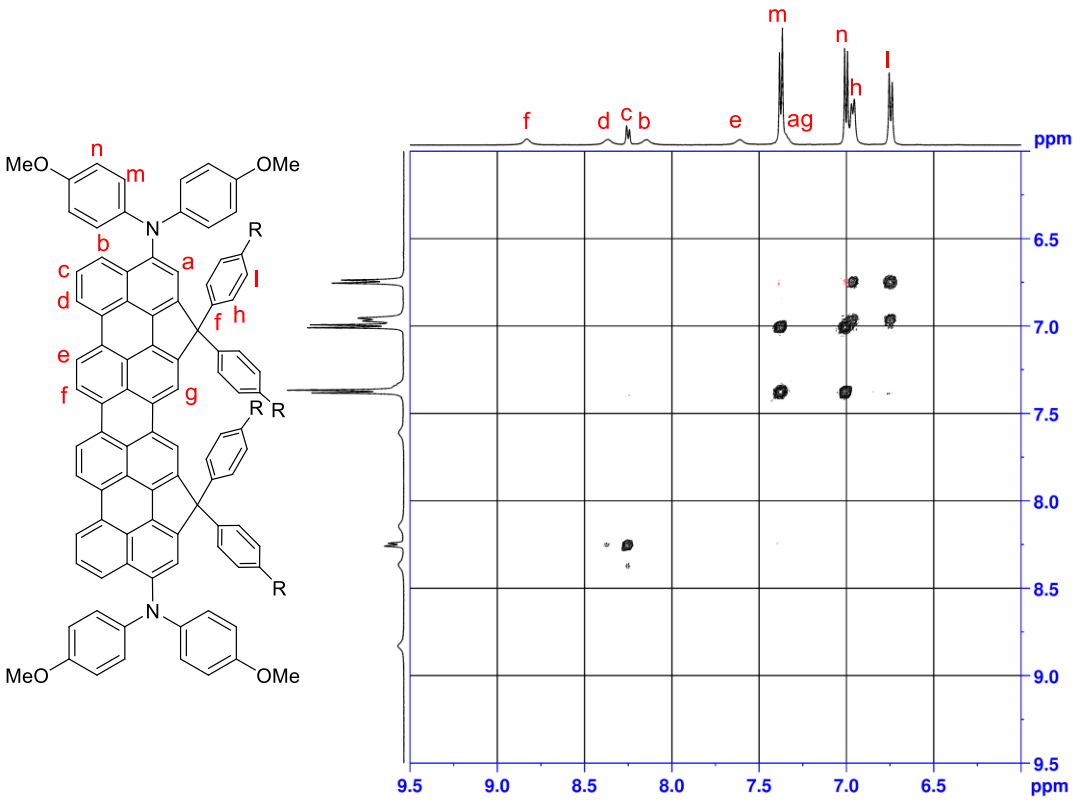

Figure S3. COSY-^{1}H NMR spectrum of compound **QR-DPN** in d_8-THF.

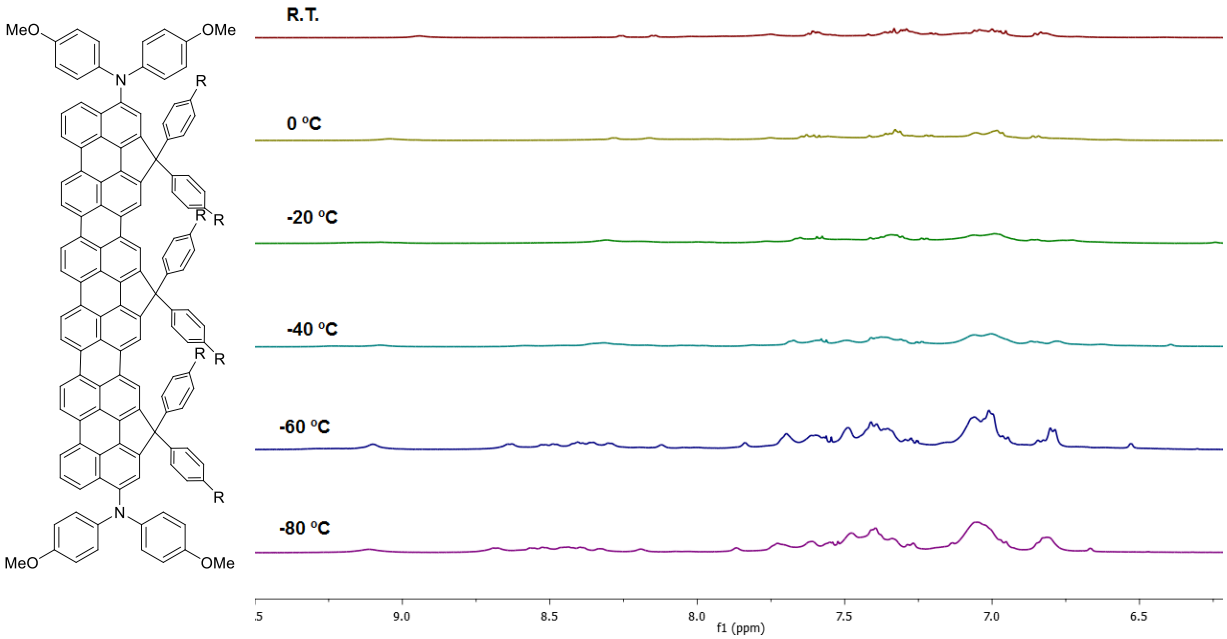

Figure S4. VT ^{1}H NMR spectra of compound **HR-DPN** in d_8-THF (500 MHz, aromatic range). The spectrum was broadened at room temperature due to thermal population from singlet ground state to the paramagnetic triple biradical, as this compound is an open-shell singlet diradicaloid (see: W. Zeng, H. Phan, T. S. Herng, T. Y. Gopalakrishna, N. Aratani, Z. Zeng, H. Yamada, J. Ding, J. Wu, Rylene Ribbons with Unusual Diradical Character, *Chem* **2017**, *2*, 81-92).

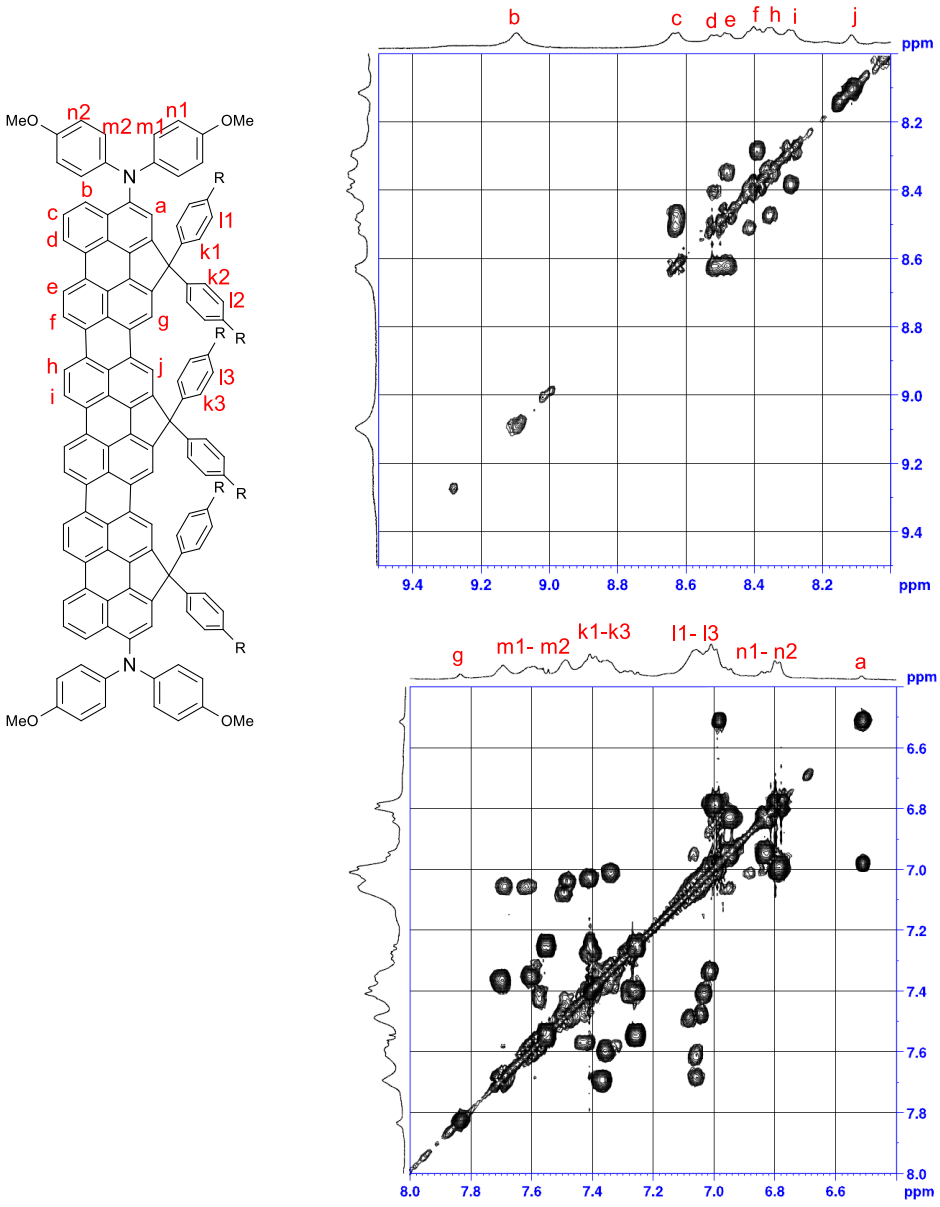

Figure S5. COSY-^{1}H NMR spectrum of compound **HR-DNP** in d_8-THF at 213 K.

Mass Spectrum SmartFormula Report

Analysis Info

Analysis Name	D:\Data\Chem\2018 Samples\201810\1019\Per-DPN.d	Acquisition Date	10/19/2018 3:58:16 PM
Method	YCH-150-1800.m	Operator	default user
Sample Name	Per-DPN	Instrument / Ser#	micrOTOF-Q II 10269
Comment	Prof Wu Jishan		

Acquisition Parameter

Source Type	APCI	Ion Polarity	Positive	Set Nebulizer	3.0 Bar
Focus	Not active	Set Capillary	4500 V	Set Dry Heater	200 °C
Scan Begin	50 m/z	Set End Plate Offset	-500 V	Set Dry Gas	6.0 l/min
Scan End	1800 m/z	Set Collision Cell RF	500.0 Vpp	Set Divert Valve	Waste

Meas. m/z	#	Formula	m/z	err [ppm]	rdb	e⁻ Conf	N-Rule
1263.7906	1	C 89 H 103 N 2 O 4	1263.7912	0.5	39.5	even	ok

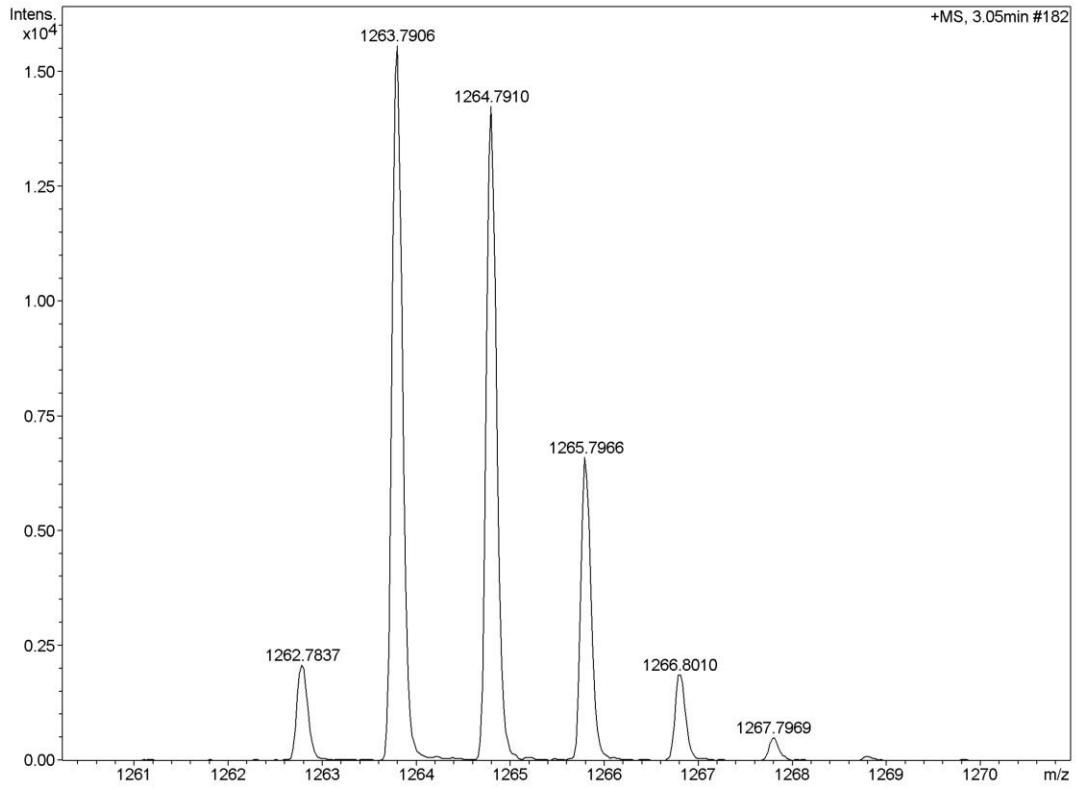

Bruker Compass DataAnalysis 4.0 printed: 10/19/2018 4:13:41 PM Page 1 of 1

Figure S6. HR mass spectrum (HPCI-HR) of the compound **1**.

Mass Spectrum SmartFormula Report

Analysis Info

Analysis Name	D:\Data\Chem\2018 Samples\201810\1019\QR-DPN-2.d	Acquisition Date	10/19/2018 5:28:17 PM
Method	YCH-1000-4000.m	Operator	default user
Sample Name	QR-DPN	Instrument / Ser#	micrOTOF-Q II 10269
Comment	Prof Wu Jishan		

Acquisition Parameter

Source Type	APCI	Ion Polarity	Positive	Set Nebulizer	3.0 Bar
Focus	Not active	Set Capillary	4500 V	Set Dry Heater	200 °C
Scan Begin	700 m/z	Set End Plate Offset	-500 V	Set Dry Gas	4.0 l/min
Scan End	4000 m/z	Set Collision Cell RF	1000.0 Vpp	Set Divert Valve	Waste

Meas. m/z	#	Formula	m/z	err [ppm]	rdb	e¯ Conf	N-Rule
2068.3558	1	C 150 H 175 N 2 O 4	2068.3546	-0.5	64.5	even	ok

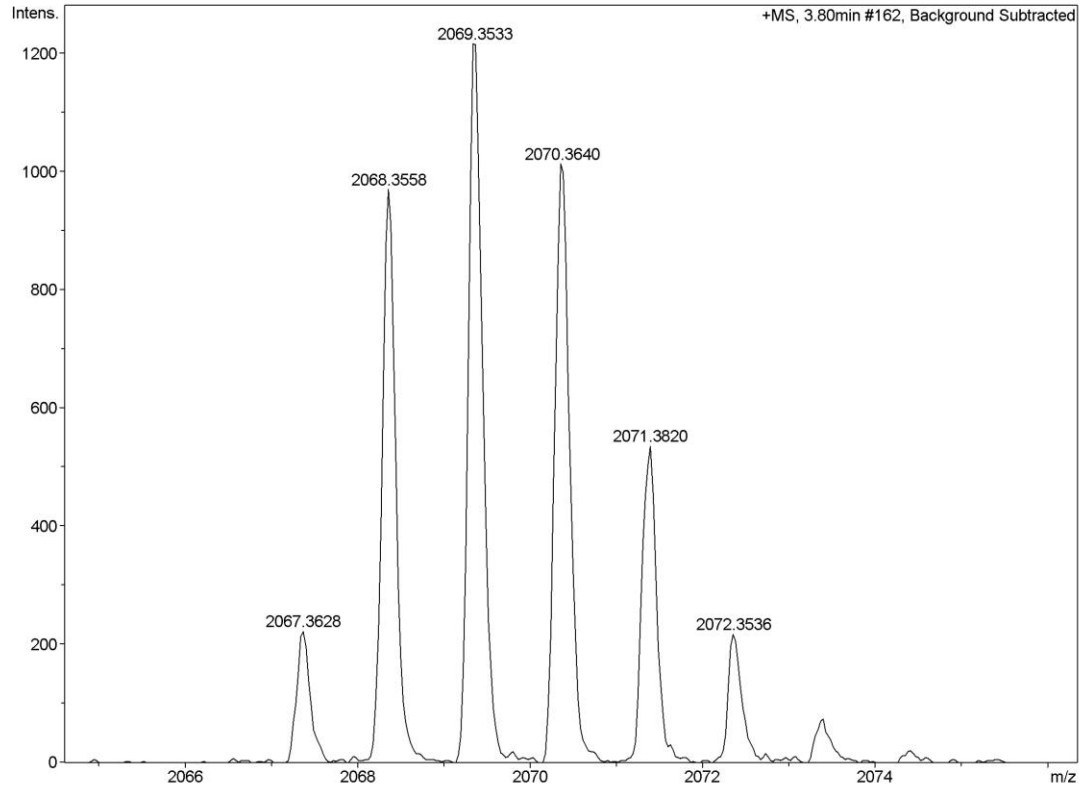

Bruker Compass DataAnalysis 4.0 printed: 10/19/2018 5:38:48 PM Page 1 of 1

Figure S7. HR mass spectrum (HPCI-HR) of the compound **QR-DPN**.

Mass Spectrum SmartFormula Report

Analysis Info

Analysis Name	D:\Data\Chem\2018 Samples\201810\1019\HR-DPN-2.d	Acquisition Date	10/22/2018 10:17:07 AM
Method	YCH-1000-4000.m	Operator	default user
Sample Name	HR-DPN	Instrument / Ser#	micrOTOF-Q II 10269
Comment	Prof Wu Jishan		

Acquisition Parameter

Source Type	APCI	Ion Polarity	Positive	Set Nebulizer	3.0 Bar
Focus	Not active	Set Capillary	4500 V	Set Dry Heater	200 °C
Scan Begin	1000 m/z	Set End Plate Offset	-500 V	Set Dry Gas	6.0 l/min
Scan End	4000 m/z	Set Collision Cell RF	1000.0 Vpp	Set Divert Valve	Waste

Meas. m/z	#	Formula	m/z	err [ppm]	rdb	e¯ Conf	N-Rule
2871.9051	1	C 211 H 246 N 2 O 4	2871.9102	1.8	90.0	odd	ok

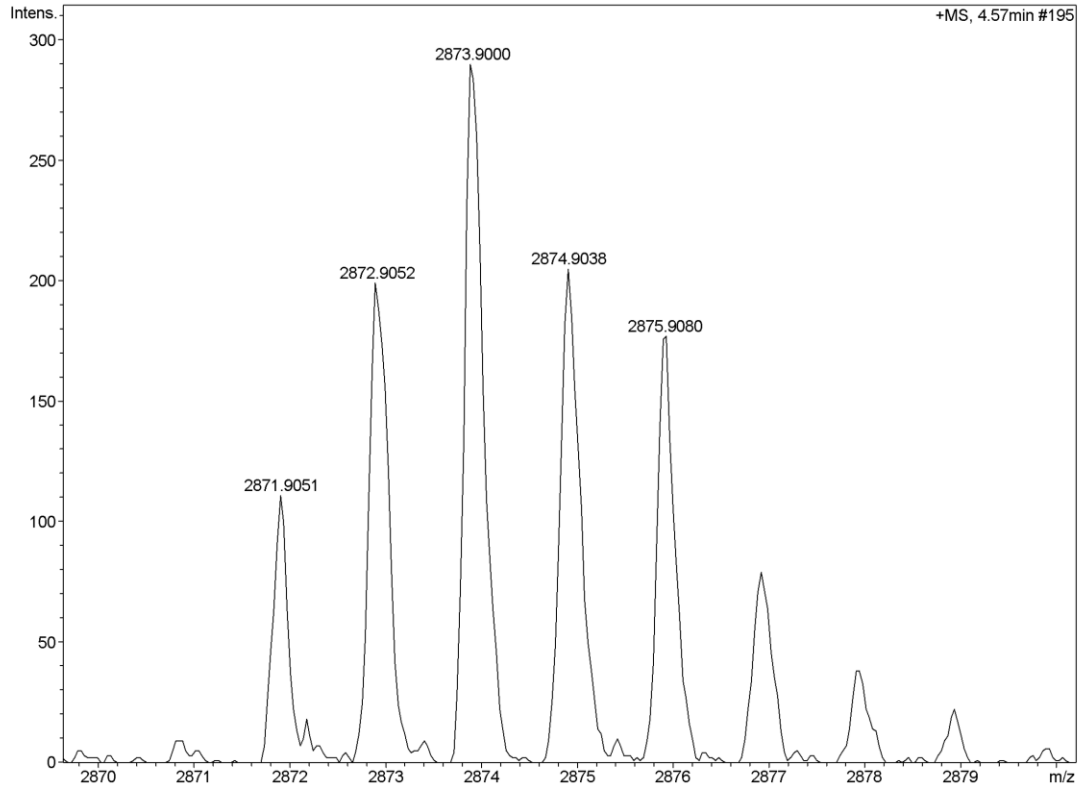

Bruker Compass DataAnalysis 4.0 printed: 10/22/2018 10:48:34 AM Page 1 of 1

Figure S8. HR mass spectrum (HPCI-HR) of the compound **HR-DPN**.

2. Electrochemistry

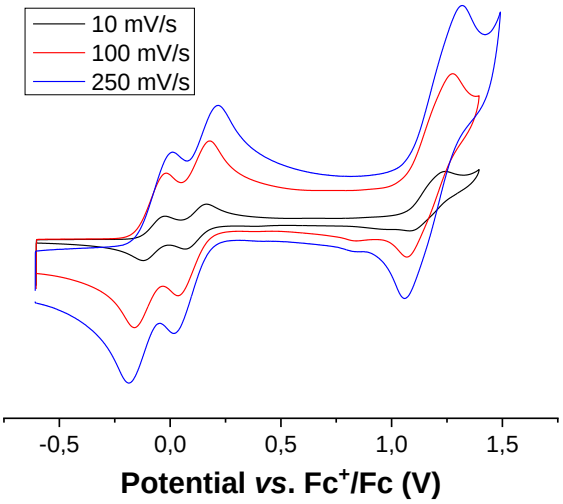

Figure S9. Cyclic voltammetry **1** (6.24×10^{-4} M, 0.03 M TBA-PF_6/o-DCB) recorded at different scan rates, in order to verify the electrochemical reversibility of the studied processes.

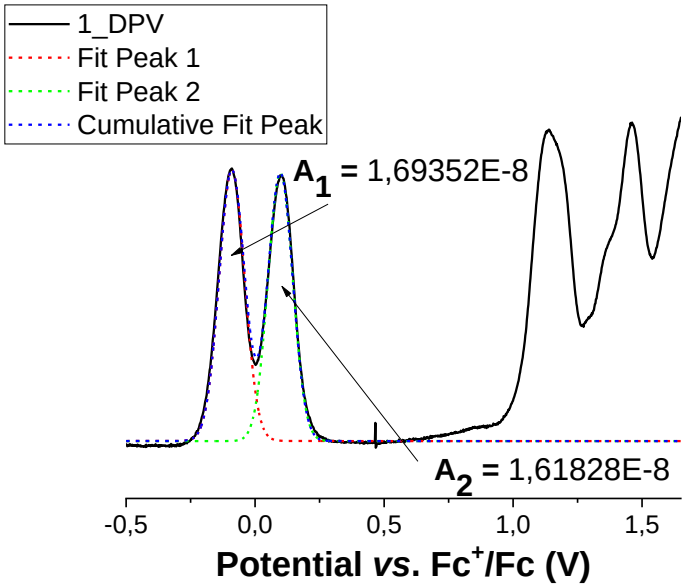

Figure S10. Differential pulse voltammetry (DPV) of **1** at a scan rate of 2 mV s^{-1}, together with the signal fitting to a Voigt model and the resulting areas.

Table S1. Fitting parameters of the DPV measurements of **1**, according to a Voigt model.

Model	Voigt	
Equation	y = nlf_voigt(x,y0,xc,A,wG,wL);	
Plot	Peak1(**1_DPV**)	Peak2(**1_DPV**)
y0	3,91E-9 ± 3,19E-10	3,90786E-9 ± 3,19E-10
xc	**-0,09 ± 2,67E-4**	**0,10 ± 2,95E-4**
A	1,69E-8 ± 3,0184E-10	1,62E-8 ± 1,07E-10
wG	0,11589 ± 0,00263	0,11272 ± 8,1919E-4
wL	6,7623E-4 ± 0,00443	7,6479E-15 ± 3,99366E-4
Reduced Chi-Sqr	1,02251E-17	
R-Square (COD)	0,99574	
Adj. R-Square	0,99565	

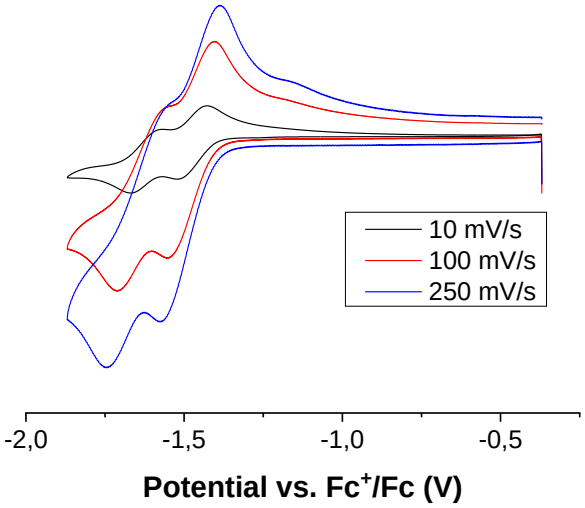

Figure S11. Cyclic voltammetry **2** (6.0E-4 M, 0.03 M TBA-PF_6/o-DCB) recorded at different scan rates, in order to verify the electrochemical reversibility of the studied processes.

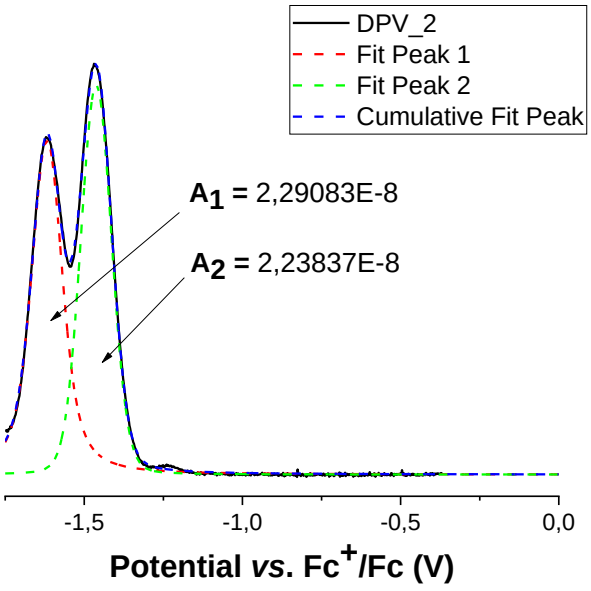

Figure S12. Differential pulse voltammetry (DPV) of **2** at a scan rate of 2 mV s^{-1}, together with the signal fitting to a Voigt model and the resulting areas.

Table S2. Fitting parameters of DPV measurements of **2**, according to a Voigt model.

Model	Voigt	
Equation	y = nlf_voigt(x,y0,xc,A,wG,wL);	
Plot	Peak1(**2_DPV**)	Peak2(**2_DPV**)
y0	9,13E-10 ± 2,04E-10	9,13E-10 ± 2,04E-10
xc	**-1,62 ± 1,56E-4**	**-1,46 ± 1,20E-4**
A	2,29E-8 ± 1,80E-10	2,24E-8 ± 1,72E-10
wG	0,0791 ± 0,00153	0,109 ± 0,00105
wL	0,05907 ± 0,00192	0,01049 ± 0,00173
Reduced Chi-Sqr	2,27541E-18	
R-Square (COD)	0,99945	
Adj. R-Square	0,99944	

3. Spectroelectrochemistry

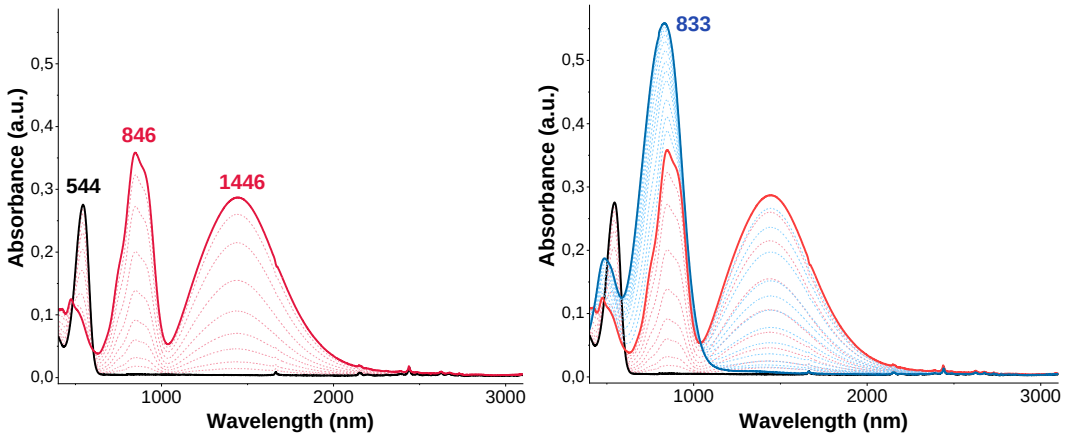

Figure S13. UV-Vis-NIR absorption spectra of **1** electrochemically oxidized (10^{-4} M, 0.02 M TBA-PF_6/o-DCB), separated by species. Neutral: black solid line; Radical cation: red solid line; Dication: blue solid line.

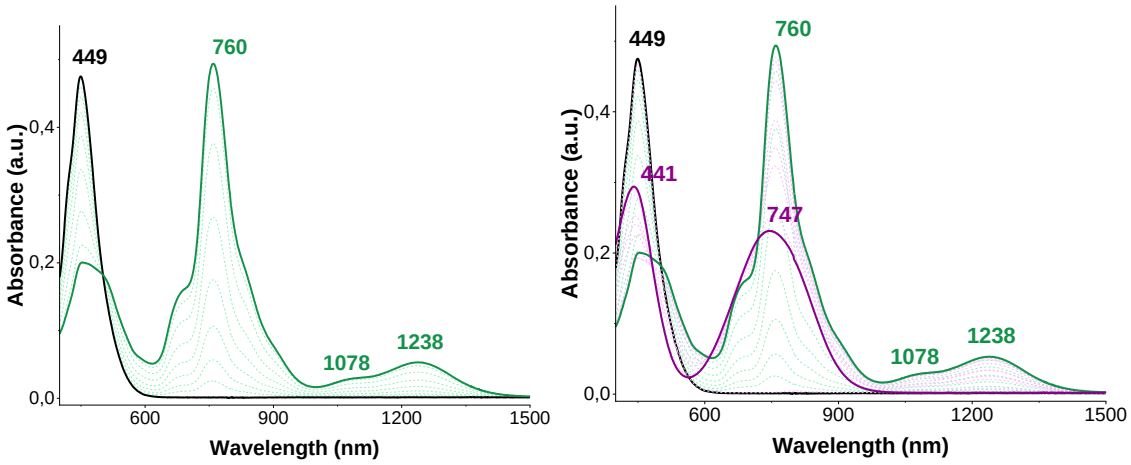

Figure S14. UV-Vis-NIR absorption spectra of **2** (10^{-4} M, 0.02 M TBA-PF_6/o-DCB) electrochemically reduced, separated by species. Neutral: black solid line; Radical anion: green solid line; Dianion: purple solid line.

4. Theoretical calculations

Geometries of Per-DPN (compound **1**) and Per-2N (compound **2**) were optimized for the neutral, radical anion (cation) and dianion (dication) forms using density functional theory. The 6-31G** basis set was employed and the B3LYP, BLYP35 and CAM-B3LYP functionals were selected. The former was used to investigate the electronic communication between the redox centers and the bridge and to evaluate intramolecular reorganization energies since it has been used previously for a wide variety of conjugated systems. Reorganization energies were computed for the redox centers, with the adiabatic potential method.[1-3] To this end the geometries of the donor (acceptor) redox centers were optimized in both neutral and charged states.

Equilibrium structures were determined at CAM-B3LYP/6-31G** and BLYP35/6-31G** level, including solvent (*o*-dichlorobenzene) described with the SCRF model in the framework of the PCM approach.[4-6] The CAM-B3LYP and BLYP35 functionals were selected since they have been shown to provide a realistic and balanced description of the localization / delocalization of charges in Robin-Day class II and III conjugated systems[7] and especially the latter has been tested on a wide variety of mixed-valence systems. [8]
In this regard we note that for the radical species we could not find asymmetric geometries with charge localized on a single redox center. Similarly, for the closed shell diradical systems, a broken symmetry solution was not found. These results show that the ground state potential energy surface of the radical species displays a single minimum in agreement with a Robin-Day class III system.

The equilibrium structures of neutral and charged species were then employed for TDDFT calculations of vertical excitation energies with the inclusion of solvent effects described with the linear response theory.[9-10] The CAM-B3LYP and BLYP35 functionals were selected to simulate the absorption spectra of neutral and charged species. For comparison with experimental absorption spectra and for the evaluation of electronic couplings between redox centers, the TD-CAM-B3LYP results were scaled by 0.3 eV to account for the known overestimate of the method.[7] The computed electronic couplings between redox centers are compared with the results from different functionals.

Electronic communication with the bridge and intra-molecular reorganization energies

To estimate electronic communication between the redox centers and the bridge, a fragment orbital approach was adopted. The fragments were frozen at the optimized geometry of the full molecule and dangling bonds were saturated with hydrogen atoms. The molecular orbitals of the fragments were determined and used, together with the results on the full molecule, to construct an orbital interaction diagram shown in Figure 3 for **1** and for **2**.

Figure 3 shows that for **2** the interaction between the HOMO of perylene and the antisymmetric combination of the orbitals of redox centers (LUMO) is large and results in a higher energy empty LUMO orbital of **2** bearing a strong parentage with the HOMO of perylene. The quinoidal structure of **2** then follows because of the emptied perylene HOMO contribution which is of aromatic character. The remarkable reorganization of orbital energies upon interaction is a manifestation of the strong electron communication between the redox centers and the bridge also for **2** and points to a Robin-Day class III system where the charge is delocalized over the entire molecule, as demonstrated by geometry optimization.

The intramolecular reorganization energy associated with the charge transfer between the two redox centers was evaluated as

$$\lambda_{(i)} = [E^n(geo_c) - E^n(geo_n)]_i + [E^c(geo_n) - E^c(geo_c)]_i = \lambda^n_{(i)} + \lambda^c_{(i)}$$

where $E^{n/c}(geo_{c/n})$ is the energy of the neutral/charged redox center at the geometry of the charged/neutral species.

The reorganization energy estimated for the amine redox center (redox center for compound **1**) agrees with previously reported values [11]

Table S3 B3LYP/6-31G** computed reorganization energies (cm^{-1}) for the DBD (**1**) and ABA (**2**) systems

Compound 1				
	λ^n		$\lambda^c = \lambda^{cation}$	$\lambda_{(a,b)}$
Redox unit 1	1246	**Redox unit 2**	1250	2496
Compound 2				
	λ^n		$\lambda^c = \lambda^{anion}$	$\lambda_{(a,b)}$
Redox unit 1	839	**Redox unit 2**	782	1621

Equilibrium structures

The most relevant computed CC and CN bond lengths for the neutral and charged species, optimized at CAM-B3LYP/6-31G** including solvent effects described by the PCM method, are collected in Figures S15-S17.

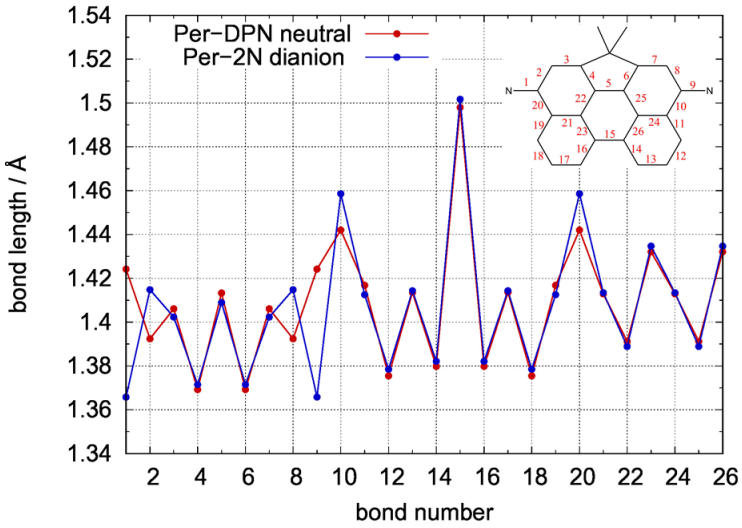

Figure S15. Comparison between CAM-B3LYP/6-31G** + PCM computed bond-lengths of Per-DPN (compound **1**) neutral and Per-2N (compound **2**) dianion.

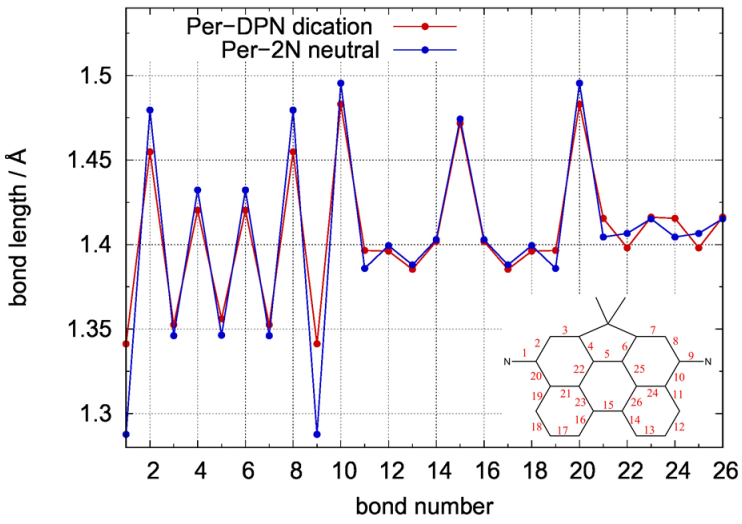

Figure S16. Comparison between CAM-B3LYP/6-31G** + PCM computed bond-lengths of Per-DPN (compound **1**) dication and Per-2N (compound **2**) neutral.

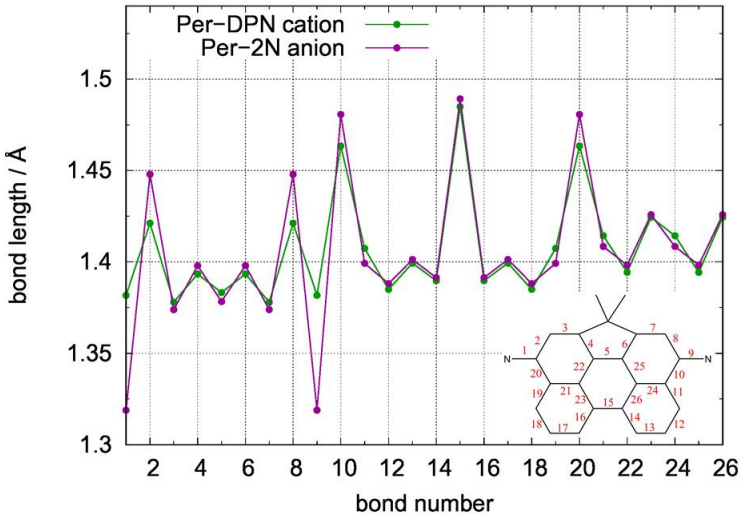

Figure S17. Comparison between CAM-B3LYP/6-31G** + PCM computed bond-lengths of Per-DPN (compound **1**) cation and Per-2N (compound **2**) anion demonstrating the similarity between the geometries.

The computed equilibrium structures of charged systems indicate full delocalization of the charge (radical) on both redox centers through the bridge, with a potential energy surface displaying therefore a single minimum, thereby demonstrating that the two investigated systems belong to Robin-Day class III.
Additionally, the data in Figure S15 show that the bond lengths of the "Per" unit in Per-DPN (compound **1**) neutral and Per-2N (compound **2**) dianion are almost identical and typical of a Perylene derivative. This indicates a full recovery of aromaticity of **1** in its dianionic form.
The data in Figure S16 show that the bond lengths of the "Per" unit in Per-DPN (compound **1**) dication and Per-2N (compound **2**) neutral are almost identical and typical of a quinoidal Perylene derivative.
Finally, the data in Figure S17 show that the bond lengths of the "Per" unit in Per-DPN (compound **1**) radical cation and Per-2N (compound **2**) radical anion are almost identical and intermediate between those of the Per-DPN (compound **1**) and Per-2N (compound **2**) neutral species, in full agreement with Scheme 2.
In addition, the flow of electrons from the perylene HOMO to the acceptor's orbitals, ultimately determines the quinoidal structure of the former in the neutral state.

Electronic absorption spectra of 1 and 2

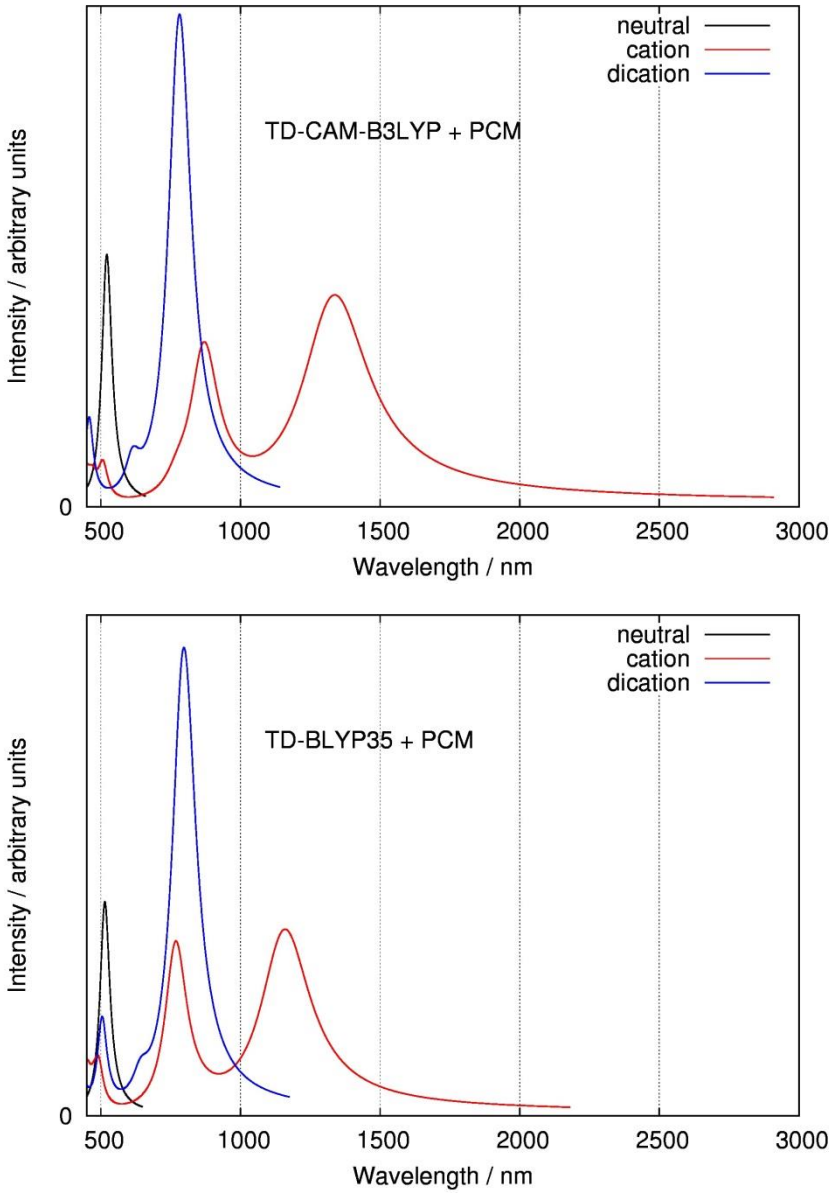

Figure S18. TD-CAM-B3LYP/6-31G** (top) and TD-BLYP35/6-31G** (bottom) predicted absorption spectra of the neutral, cationic and dicationic species of **1**, including *o*-dichlorobenzene solvent described with PCM. TD-CAM-B3LYP/6-31G** excitation energies were red-shifted by 0.3 eV in agreement with previous studies [7]. To facilitate comparison with experiment, all computed vertical excitations were broadened with a Lorentzian linewidth of 0.2 eV.

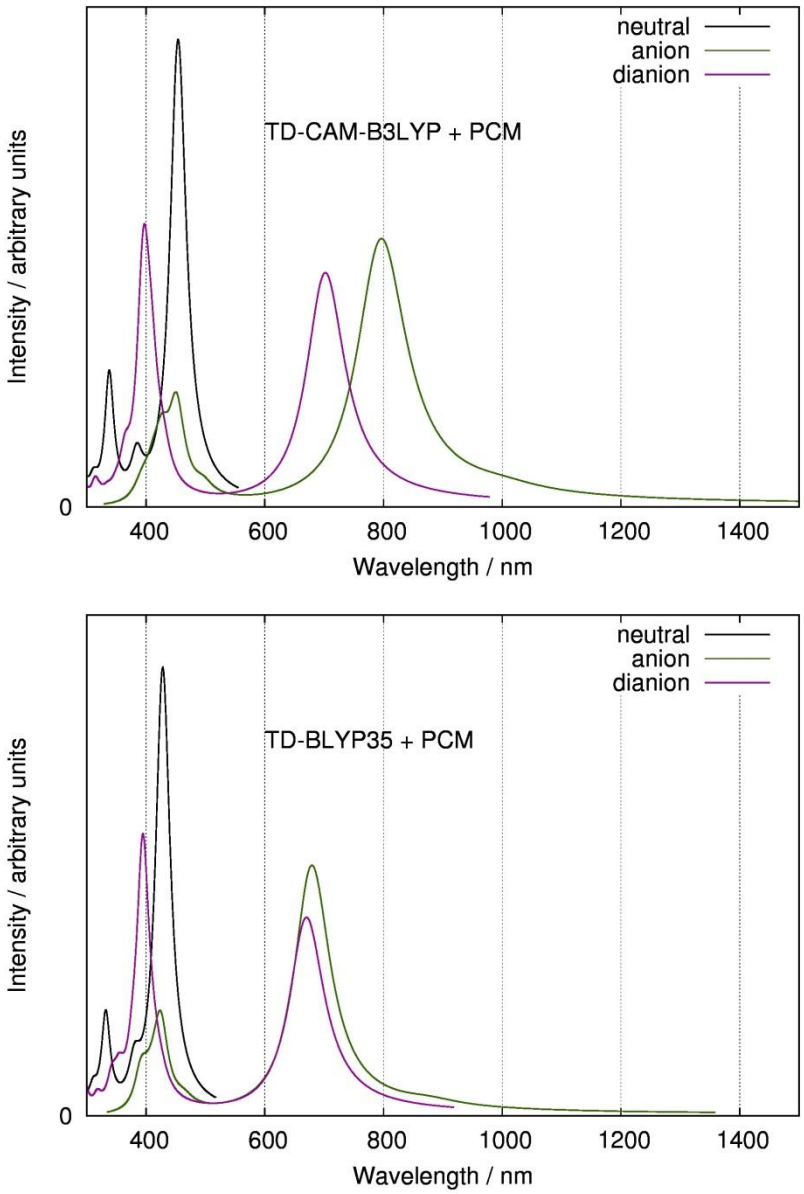

Figure S19. TD-CAM-B3LYP/6-31G** (top) and TD-BLYP35/6-31G** (bottom) predicted absorption spectra of the neutral, cationic and dicationic species of **2**, including *o*-dichlorobenzene solvent described with PCM. TD-CAM-B3LYP/6-31G** excitation energies were red-shifted by 0.3 eV in agreement with previous studies [7]. To facilitate comparison with experiment, computed vertical excitations were broadened with a Lorentzian linewidth of 0.2 eV.

The simulated absorption spectra agree with the observed counterparts (see Figures S18 and S19) for all the species investigatd (neutral, charged, douply charged) and allow the identification of the IV-CT band in the spectra of the radicals of **1** and **2** as shown in Table S4.

The lowest energy excited state for both radical ions of **1** and **2** corresponds to excitation into the IV-CT band. Therefore we extracted the electronic coupling between redox centers from the computed vertical excitation as $2V_{AB} = E(D_0 \rightarrow D_1)$. For comparison we include the estimate from different functionals (see Table S5).

Table S4. TD-UDFT/6-31G** computed excitation energies (E), oscillator strength (f) and wavefunction (wf) for the radical ions of **1** and **2**

1				
	TD-UBLYP35 + PCM	TD-UCAM-B3LYP + PCM	TD-UB3LYP vacuo	
	E/eV (f)[a]	E/eV (f)[a]	E/eV (f)[a]	wf[b]
$D_0 \rightarrow D_1$	1.07 (0.57)	1.23 (0.64)	0.94 (0.34)	H-1→H
$D_0 \rightarrow D_2$	1.61 (0.04)	1.90 (0.05)	1.40 (0.02)	H-2→H
$D_0 \rightarrow D_3$	1.61 (0.49)	1.72 (0.48)	1.59 (0.50)	H→L
2				
	E/eV (f)	E/eV (f)	E/eV (f)	wf
$D_0 \rightarrow D_1$	1.41 (0.02)	1.54 (0.02)	1.25 (0.01)	L→L+1
$D_0 \rightarrow D_2$	1.83 (0.84)	1.86 (0.84)	1.90 (0.61)	H→L

[a]unscaled excitation energies [b]orbital labels refer to the occupation in the neutral molecule

Table S5. Computed electronic couplings between the redox centers of **1** and **2**.

1			
	$E(D_0 \rightarrow D_1)/eV$	Wf[a]	V_{AB}/cm^{-1}
TD-UBLYP35 +PCM	1.07	H-1→H	4315
TD-UCAM-B3LYP +PCM	1.23	H-1→H	4960
TD-UB3LYP	0.94	H-1→H	3790
2			
	$E(D_0 \rightarrow D_1)/eV$	Wf[a]	V_{AB}/cm^{-1}
TD-UBLYP35 +PCM	1.41	L→L+1	5686
TD-UCAM-B3LYP +PCM	1.54	L→L+1	6210
TD-UB3LYP	1.25	L→L+1	5040

[a]the orbital labels refer to the occupation in the neutral molecule

References for the computational section

1 J.-L. Bredas, D. Beljonne, V. Coropceanu, J. Cornil, "Charge-Transfer and Energy-Transfer Processes in pi-Conjugated Oligomers and Polymers: A Molecular Picture", *Chem. Rev.* **2004**, *104*, 4971-5003.

2 V. Coropceanu, J. Cornil, D. A. da Silva, Y. Olivier, R. Silbey, J.-L. Bredas, "Charge Transport in Organic Semiconductors", *Chem. Rev.* **2007**, *107*, 926-952.

3 H. Oberhofer, K. Reuter, J. Blumberger, "Charge Transport in Molecular Materials: An Assessment of Computational Methods", *Chem. Rev.* **2017**, *117*, 10319-10357.

4 M. Cossi, V. Barone, R. Cammi, J. Tomasi, *Chem. Phys. Lett.* **1996**, *255*, 327-335.

5 B. Mennucci, J. Tomasi, *J. Chem. Phys.* **1997**, *106*, 5151-5158

6 J. Tomasi, R. Cammi, B. Mennucci, C. Cappelli, S. Corni, *Phys. Chem. Chem. Phys.* **2002**, *4*, 5697-5712

7 W. Jiang, C. Xiao, L. Hao, Z. Wang, H. Ceymann, C. Lambert, S. Di Motta, F. Negri, "Localization/Delocalization of Charges in Bay-Linked Perylene Bisimides", *Chem. Eur. J.* **2012**, *18*, 6764-6775

8 M. Parthey, M. Kaupp, "Quantum-chemical insights into mixed-valence systems: within and beyond the Robin–Day scheme", *Chem. Soc. Rev.* **2014**, *43*, 5067-5088.

9 M. Cossi and V. Barone, Time-dependent density functional theory for molecules in liquid solutions, *J. Chem. Phys.* **2001**, *115*, 4708-4717.

10 R. Cammi and B. Mennucci, Linear response theory for the polarizable continuum model, *J. Chem. Phys.* **1999**, *110*, 9877-9886.

11 A. V. Szeghalmi, M. Erdmann, V. Engel, M. Schmitt, S. Amthor, V. Kriegisch, G. Nöll, R. Stahl, C. Lambert, D. Leusser, D. Stalke, M. Zabel, J. Popp, *J. Am. Chem. Soc.* **2004**, *126*, 7834-7845.

5. Mathematical Treatment of the IV-CT band of the MV compounds

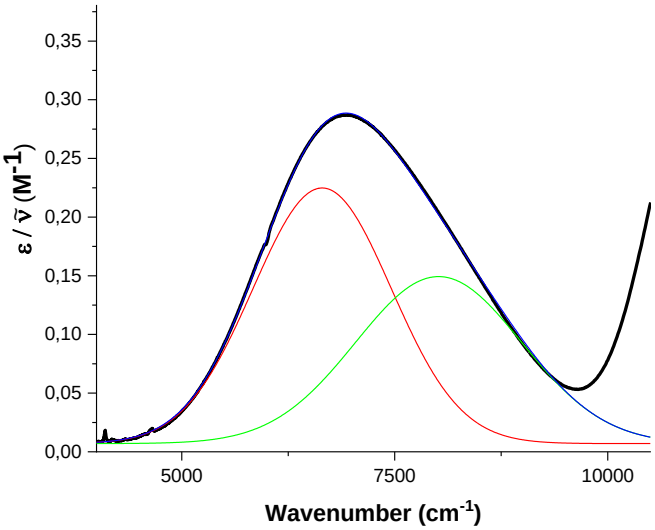

Figure S20. Selected section containing the lowest energy absorption bands of the reduced spectrum of **1**$^{\bullet+}$ and fitting of IV-CT according to a GaussAmp function.

Table S6. Fitting parameters of the IV-CT band of the radical cation (RC) of **1**, according to a GaussAmp function. Every peak has been highlighted matching the scheme colour of Figure S20.

Model	GaussAmp	
Equation	y=y0+A*exp(-0.5*((x-xc)/w)^2)	
Plot	Peak1(1_RC)	Peak2(1_RC)
y0	0,007 ± 1,77067E-4	0,007 ± 1,77067E-4
xc	6648,25028 ± 10,73062	8015 ± 31,47594
w	811,49105 ± 3,87657	974,32308 ± 13,05107
A	0,21782 ± 0,00503	0,14231 ± 0,00306
Reduced Chi-Sqr	3,50095E-6	
R-Square (COD)	0,99964	
Adj. R-Square	0,99964	

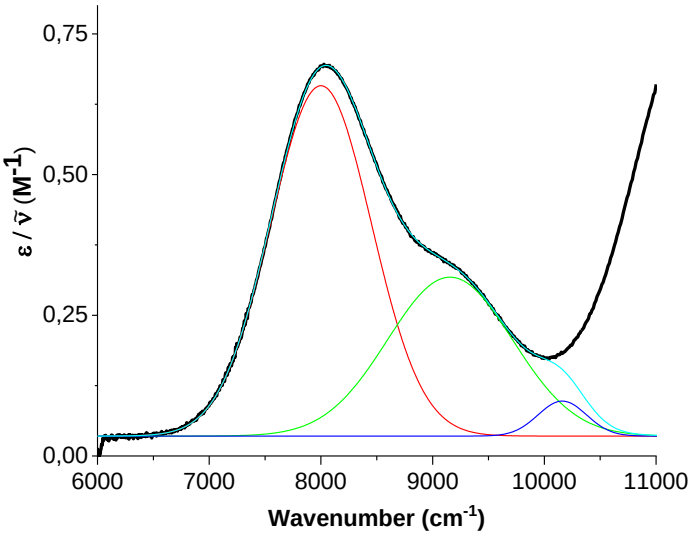

Figure S21. Selected section containing the lowest energy absorption bands of the reduced spectrum of **2**$^{\bullet-}$ and fitting of IV-CT according to a GaussAmp function.

Table S7. Fitting parameters of the IV-CT band of the radical anion (RA) of **2**, according to a GaussAmp function. Every peak has been highlighted matching the scheme colour of Figure S21.

Model	GaussAmp		
Equation	y=y0+A*exp(-0.5*((x-xc)/w)^2)		
Plot	Peak1(2_RA)	Peak2(2_RA)	Peak3(2_RA)
y0	0,03536 ± 1,87911E-4	0,03536 ± 1,87911E-4	0,03536 ± 1,87911E-4
xc	8000,17295 ± 1,72856	9155,94174 ± 3,33199	10160,62502 ± 128,48501
w	452,13222 ± 0,82437	558,98133 ± 6,65914	216,43858 ± 52,55561
A	0,62255 ± 0,00215	0,28237 ± 4,827E-4	0,06228 ± 0,02515
Reduced Chi-Sqr	5,27385E-6		
R-Square (COD)	0,9999		
Adj. R-Square	0,99989		

6. Longer members of the bis(diarylamine) and bis(diimine) series

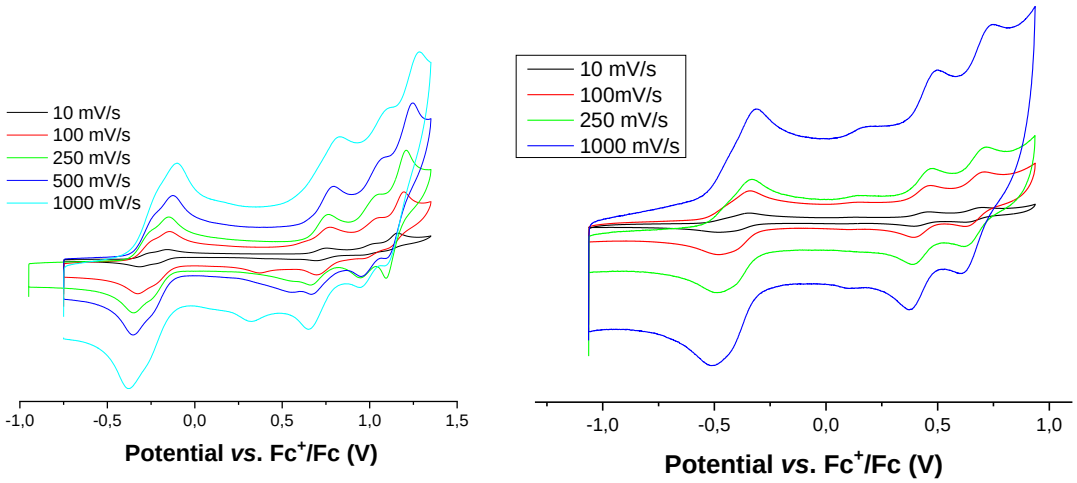

Figure S22. Cyclic voltammetry of **QR-DPN** (left) and **HR-DPN** (right) (10^{-4} M, 0.03 M TBA-PF_6/o-DCB) recorded at different scan rates, in order to verify the electrochemical reversibility of the studied processes.

Table S7. Electrochemical data (V vs. Fc^+/Fc) for the oxidation processes of of **QR-DPN** and **HR-DPN** measured by OSWV in 10^{-4} M, 0.03 M TBA-PF_6/o-DCB

o-DCB (0.03 M)	$E_{1/2}^{ox1}$ (V)	$E_{1/2}^{ox2}$ (V)	$E_{1/2}^{ox3}$ (V)	$E_{1/2}^{o4}$ (V)	$E_{1/2}^{ox5}$ (V)
QR-DPN	-0.33	-0.24	0.67	0.95	1,07
HR-DPN	-0,46	-0.37	0.43	0.67	1,02 (*)

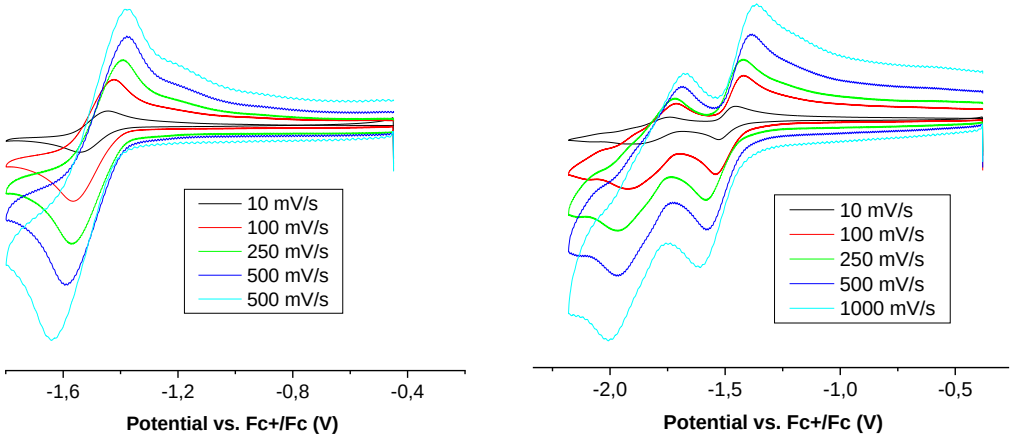

Figure S23. Cyclic voltammetry of **QR-2N** (left) and **HR-2N** (right) (10^{-4} M, 0.03 M TBA-PF_6/o-DCB) recorded at different scan rates, in order to verify the electrochemical reversibility of the studied processes.

Table S8. Electrochemical data (V vs. Fc^+/Fc) for the reduction processes of of **QR-2N** and **HR-2N** measured by OSWV in 10^{-4} M, 0.03 M TBA-PF_6/o-DCB

o-DCB (0.03 M)	QR-2N	HR-2N
$E_{1/2}^{red1}$ (V)	-1.48 ($2e^-$)	-1,48 ($2e^-$)

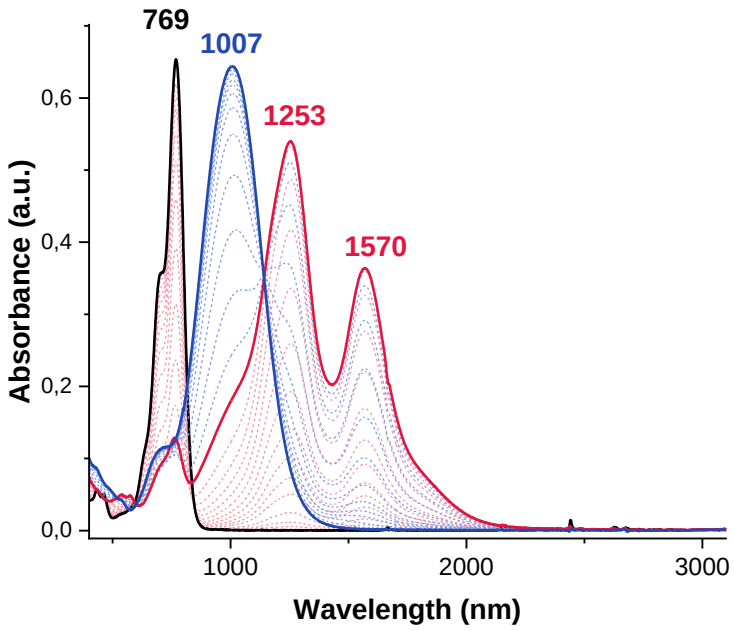

Figure S24. UV-Vis-NIR absorption spectra of **QR-DPN** electrochemically oxidized (10^{-4} M, 0.02 M TBA-PF_6/o-DCB). Neutral: black solid line; Radical cation: red solid line; Dication: blue solid line.

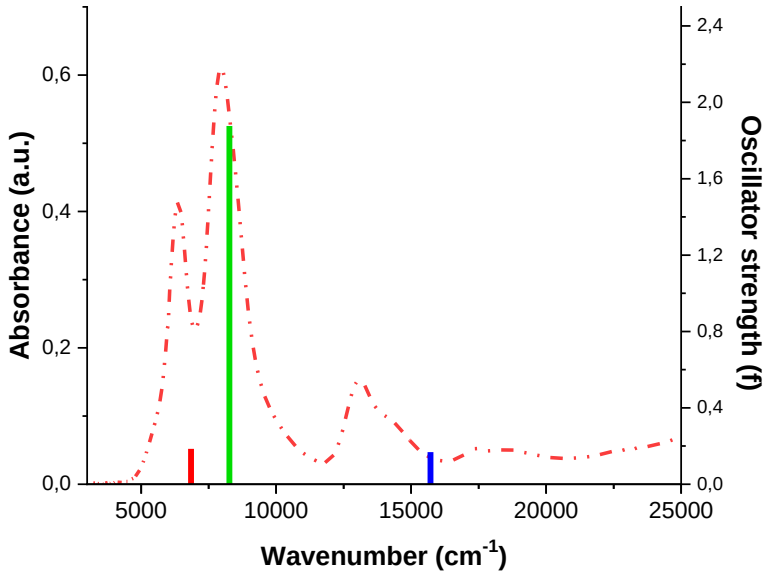

Figure S25. Reduced absorption spectra of **QR-DPN**$^{\bullet+}$ with its respective calculated results from TD-DFT// UBLYP35/SVP, including o-DCB solvent described with PCM.

```
Excited State   1:   2.045-?Sym     0.8490 eV 1460.32 nm  f=0.1855  <S**2>=0.796
    270A -> 273A       -0.13153
    271A -> 274A        0.11859
    272A -> 273A        0.89380
    269B -> 272B       -0.14138
    271B -> 272B        0.37875
    272A <- 273A        0.12338
```

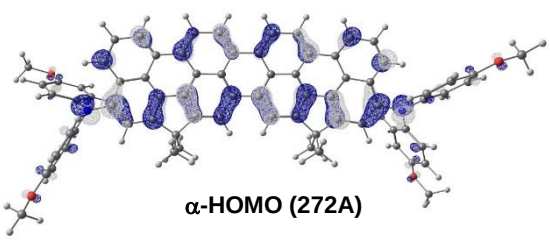

α-HOMO (272A)

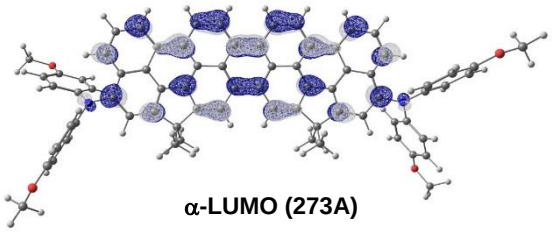

α-LUMO (273A)

```
Excited State   2:   2.215-?Sym     1.0253 eV 1209.19 nm  f=1.8762  <S**2>=0.977
    270A -> 273A        0.11955
    272A -> 273A       -0.33204
    270B -> 273B       -0.23184
    271B -> 272B        0.87952
```

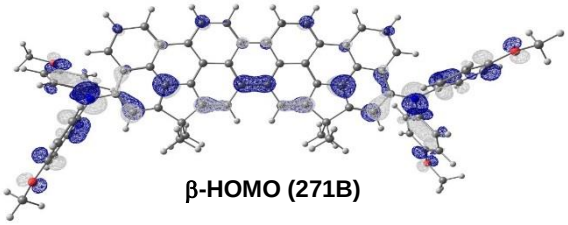

β-HOMO (271B)

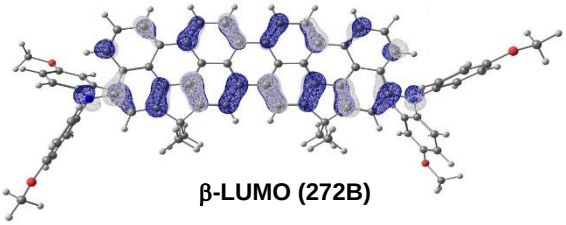

β-LUMO (272B)

Figure S26. Calculated topologies (UBLYP35/SVP, CPCM, Solvent=o-DCB) of the orbitals of **QR-DPN**$^{\bullet+}$ related to the major contributions of the main bands of the reduced absorption spectrum. (A) = (α) and (B) = (β).

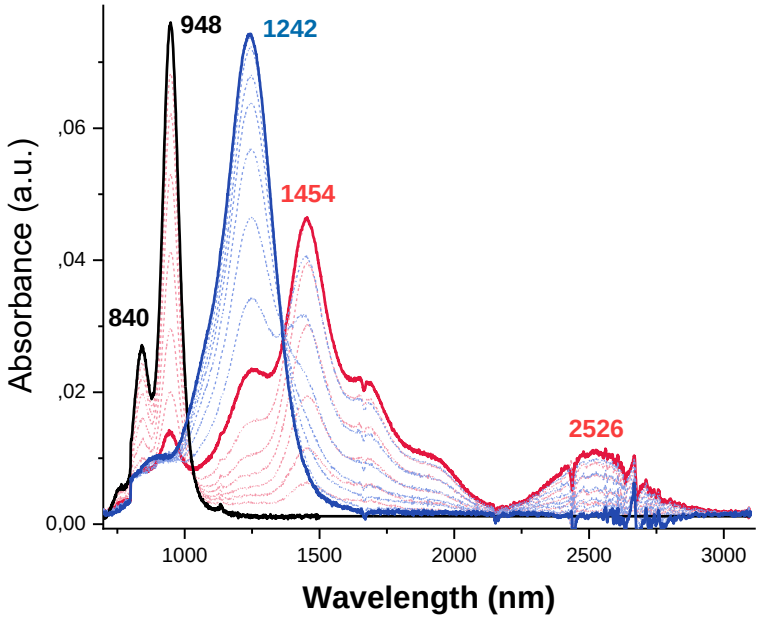

Figure S27. UV-Vis-NIR absorption spectra of **HR-DPN** electrochemically oxidized (10^{-4} M, 0.02 M TBA-PF_6/o-DCB). Neutral: black solid line; Radical cation: red solid line; Dication: blue solid line.

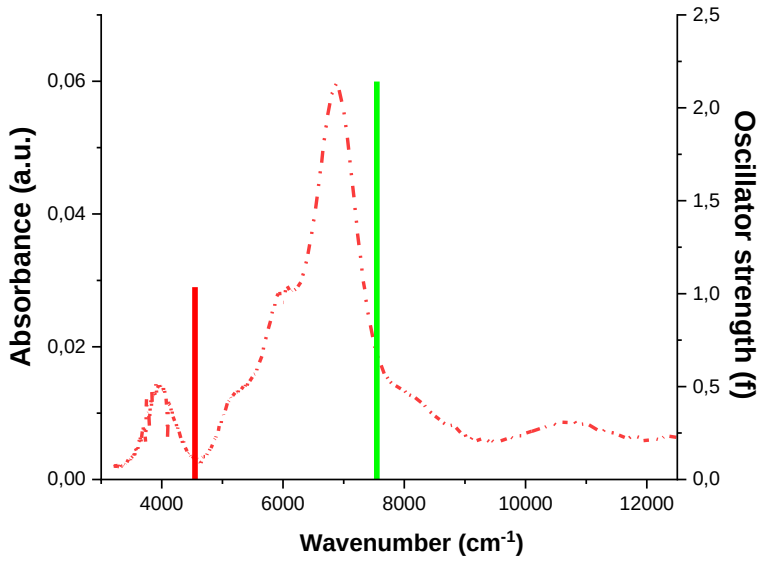

Figure S28. Reduced absorption spectra of **HR-DPN**$^{\bullet+}$ with its respective calculated results from TD-DFT// UBLYP35/SVP, including o-DCB solvent described with PCM.

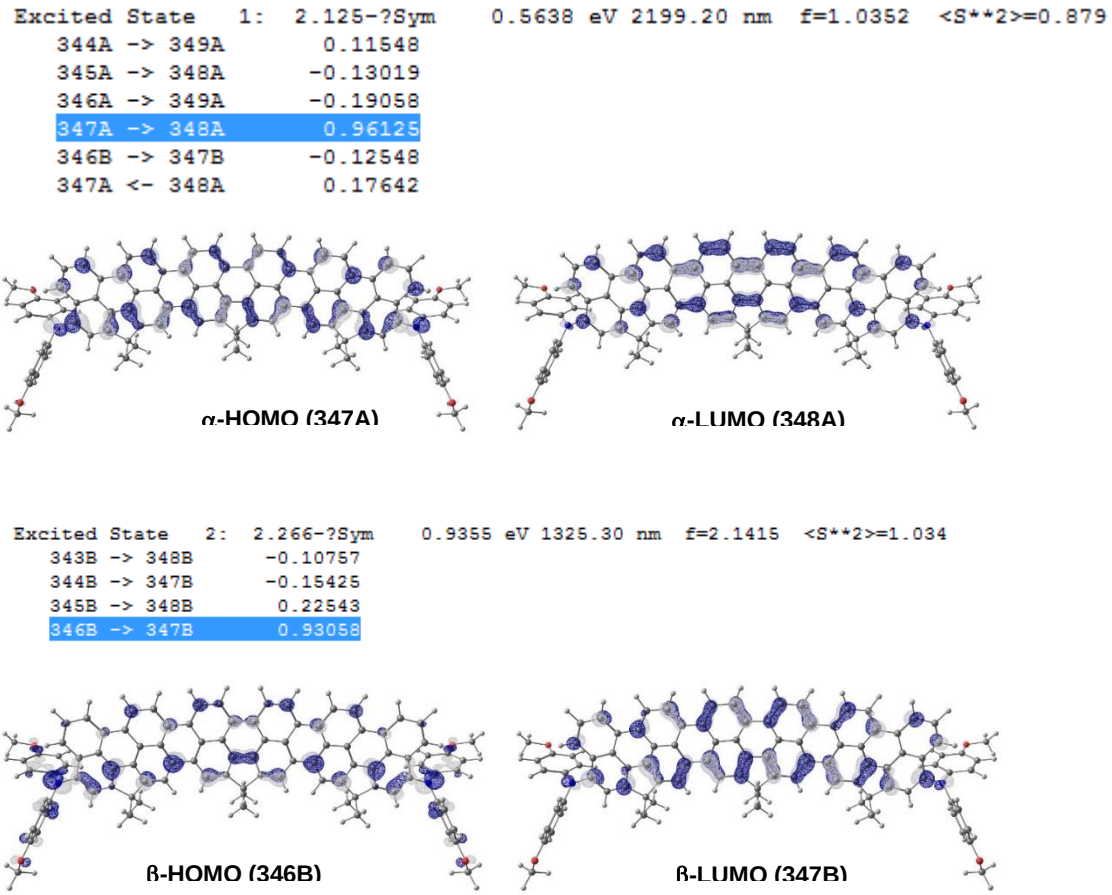

Figure S29. Calculated topologies (UBLYP35/SVP, CPCM, Solvent=o-DCB) of the orbitals of **HR-DPN**$^{\bullet+}$ related to the major contributions of the main bands of the reduced absorption spectrum. (A) = (α) and (B) = (β).

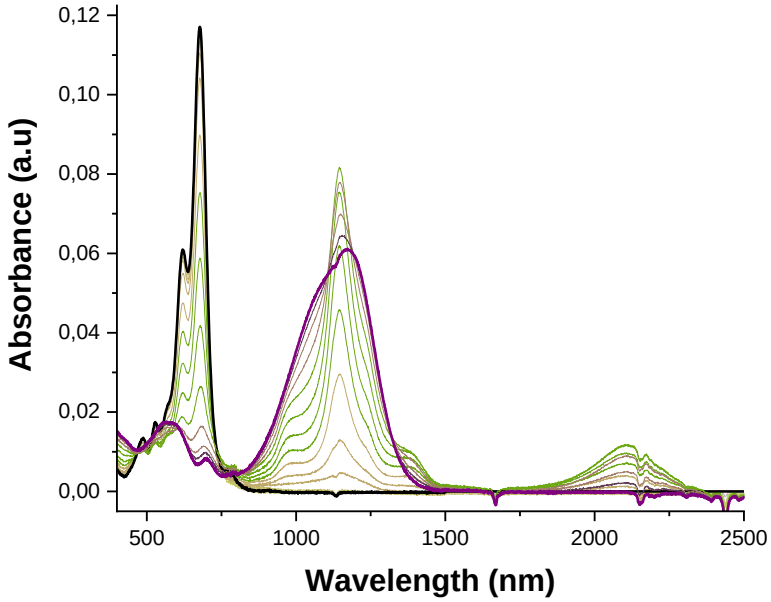

Figure S30. UV-Vis-NIR absorption spectra of **QR-2N** electrochemically reduced (10^{-4} M, 0.02 M TBA-PF_6/o-DCB). Neutral: black solid line; Dianion: purple solid line.

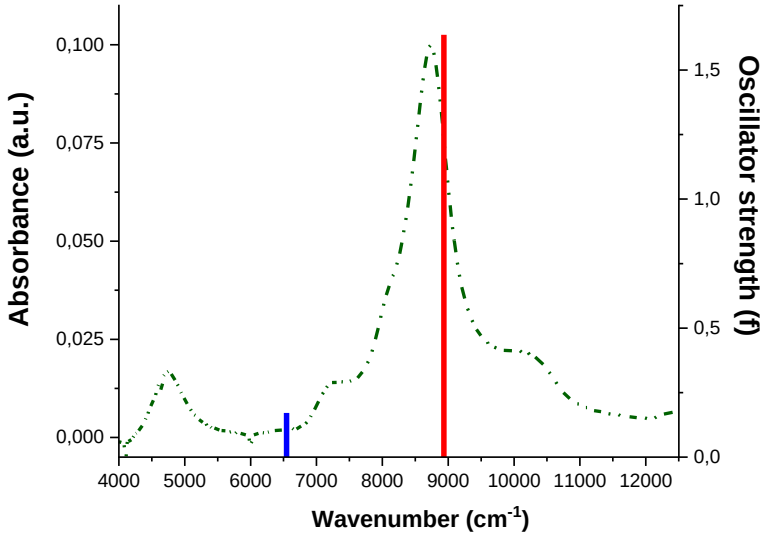

Figure S31. Reduced absorption spectra of pure **QR-2N**$^{\bullet-}$ obtained from Specfit software, together with its respective calculated results from TD-DFT// UBLYP35/SVP, including o-DCB solvent described with PCM.

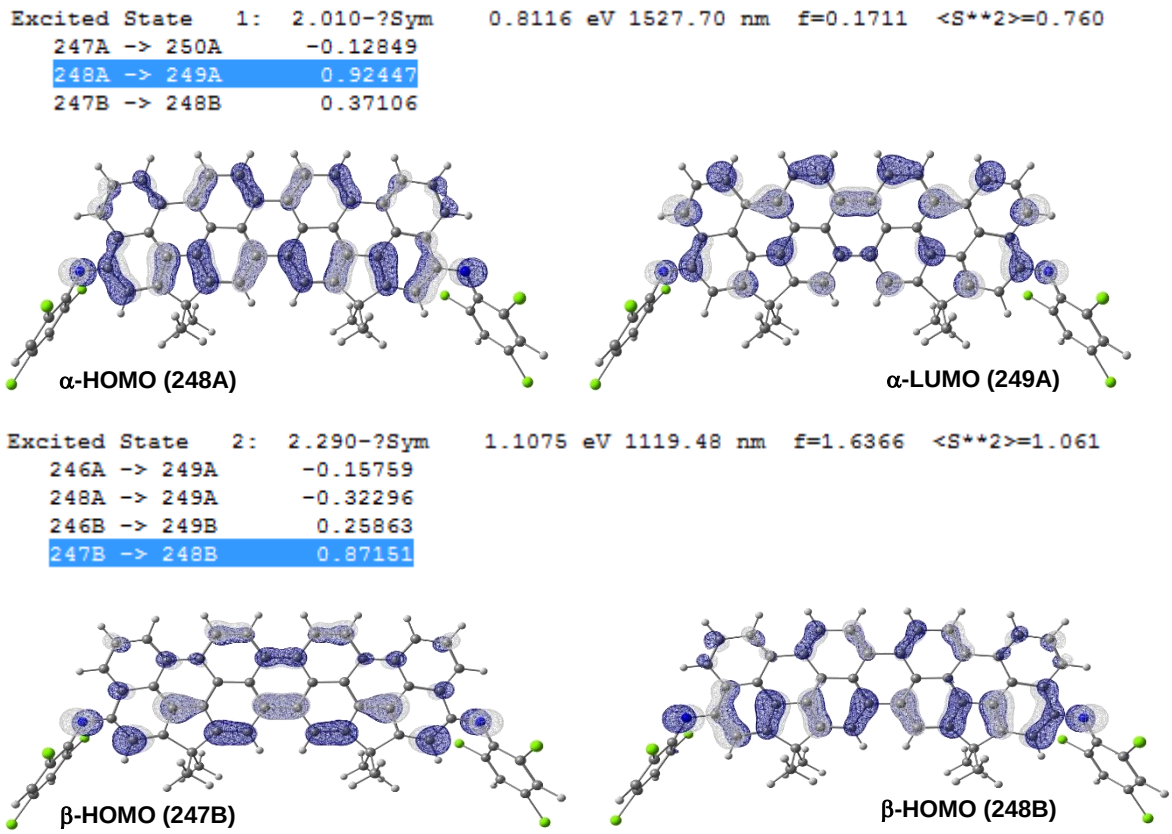

Figure S32 Calculated topologies (UBLYP35/SVP, CPCM, Solvent=o-DCB) of the orbitals of **QR-2N**$^{\bullet-}$ related to the major contributions of the main bands of the reduced absorption spectrum. (A) = (α) and (B) = (β).

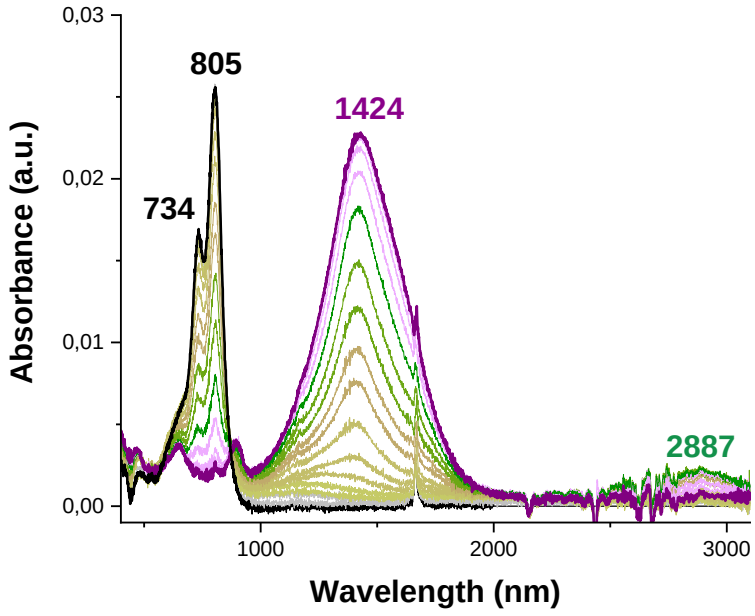

Figure S33. UV-Vis-NIR absorption spectra of **HR-2N** electrochemically reduced (10^{-4} M, 0.02 M TBA-PF_6/o-DCB). Neutral: black solid line; Dianion: purple solid line.

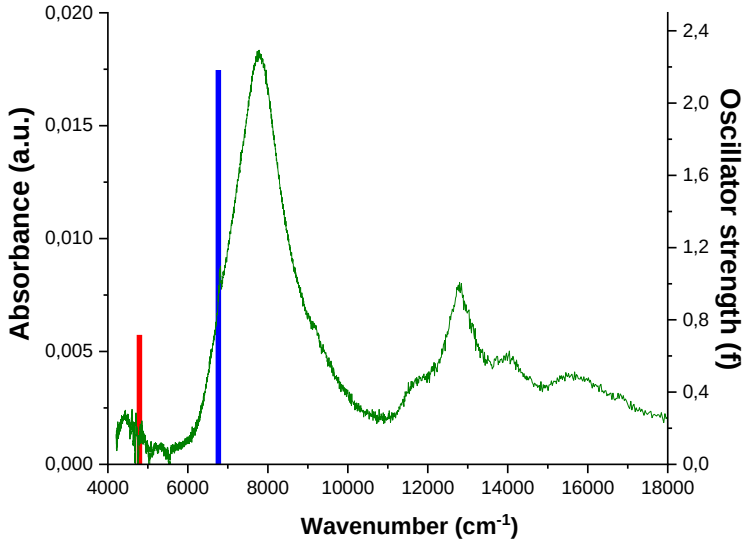

Figure S34. Reduced absorption spectra of pure **HR-2N$^{\bullet-}$** obtained from Specfit software, together with its respective calculated results from TD-DFT// UBLYP35/SVP, including o-DCB solvent described with PCM.

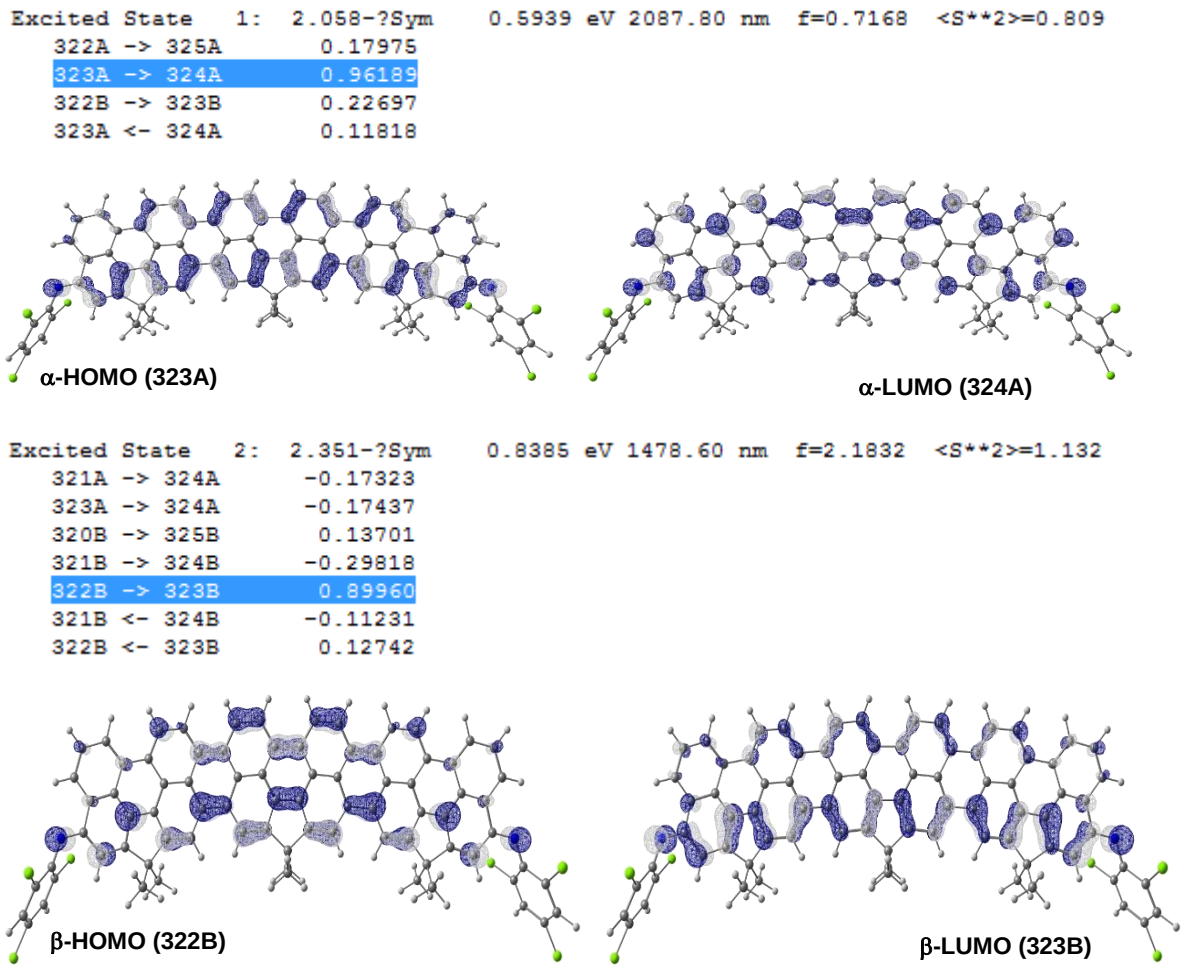

Figure S35. Calculated topologies (UBLYP35/SVP, CPCM, Solvent=o-DCB) of the orbitals of **HR-2N$^{\bullet-}$** related to the major contributions of the main bands of the reduced absorption spectrum. (A) = (α) and (B) = (β).

7 EPR simulations

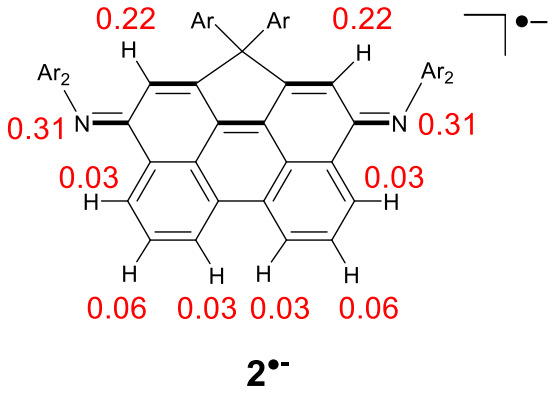

Figure S36. Isotropic hyperfine coupling constants (hcc) used for the ESR simulation for **2**$^{\bullet-}$.

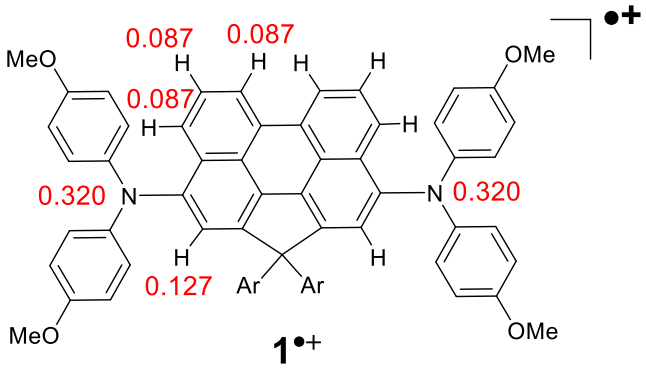

Figure S37. Isotropic hyperfine coupling constants (hcc) used for the ESR simulation for **1**$^{\bullet+}$.